



**Photoexcited charge manipulation in conjugated polymers
bearing a Ru(II) complex catalyst for visible-light CO₂
reduction**

Journal:	<i>Journal of Materials Chemistry A</i>
Manuscript ID	TA-COM-03-2022-002183.R1
Article Type:	Paper
Date Submitted by the Author:	30-Apr-2022
Complete List of Authors:	Nakada, Akinobu; Chuo University Faculty of Science and Engineering Graduate School of Science and Engineering, Department of Chemistry Miyakawa, Ryuichi; Chuo University Faculty of Science and Engineering Graduate School of Science and Engineering, Department of Chemistry Itagaki, Ren; Chuo University Faculty of Science and Engineering Graduate School of Science and Engineering, Department of Chemistry Kato, Kosaku; Toyota Technological Institute, Takashima, Chinami; Waseda University Saeki, Akinori; Osaka University, Department of Applied Chemistry, Graduate School of Engineering Yamakata, Akira; Toyota Technological Institute, Graduate School of Engineering Abe, Ryu; Kyoto University, Graduate School of Engineering Nakai, Hiromi; Waseda University, Department of Chemistry and Biochemistry Chang, Ho-Chol; Chuo University, Department of Applied Chemistry, Faculty of Science & Engineering

ARTICLE

Photoexcited charge manipulation in conjugated polymers bearing a Ru(II) complex catalyst for visible-light CO₂ reduction

Akinobu Nakada,^{*a,b} Ryuichi Miyakawa,^a Ren Itagaki,^a Kosaku Kato,^c Chinami Takashima,^d Akinori Saeki,^e Akira Yamakata,^c Ryu Abe,^f Hiromi Nakai,^{d,g,h} and Ho-Chol Chang^{*a}

Received 00th January 20xx,
Accepted 00th January 20xx

DOI: 10.1039/x0xx00000x

Conjugated polymers have emerged as a promising candidate of photocatalyst materials. Design principle, that maximizes the synergy between conjugated skeleton and catalyst moiety, is strongly desired to be established for achieving efficient photocatalysis. Herein, photoexcited charge manipulation was demonstrated by molecular engineering in conjugated polymers bearing a Ru(II) complex as the CO₂ reduction photocatalyst. Combinational studies based on ultrafast spectroscopies and theoretical calculation revealed that the introduction of an electron-donating carbazole (Cz) skeleton in the polymer enables enhanced photoexcited charge trapping on the Ru(II)-complex catalyst moiety. The carbazole-based polymer [Cz-bpyRu]_n facilitates CO₂ reduction even under visible light longer than 500 nm, and exhibited 7- to 15-folds greater activity than those of phenyl (Ph) and benzothiadiazole (Bt) counterparts. The findings of this study thus provide insights into molecular engineering for photoexcited charge manipulation to achieve efficient photocatalysis.

Introduction

Reductive conversion of CO₂ into energy-added molecules has been an important subject in the various fields including materials chemistry,^{1, 2} catalysis,^{3, 4} electrochemistry,^{5, 6} and photochemistry,^{7, 8} from viewpoints of both decreasing CO₂ concentration and gaining energy and carbon resources.⁹⁻¹¹ In particular, development of photocatalyst materials, which facilitate CO₂ reduction without high temperature and/or pressure, has been regarded as a promising way.^{7, 8}

For the past four decades, molecular-based photocatalysts including metal complexes^{12, 13} and semiconductor-based photocatalysts including metal oxides¹⁴⁻¹⁶ and mixed-anion

materials^{16, 17} have been extensively studied. High selectivity of CO₂ reduction, based on well-defined and tunable active sites, is one of the advantages of molecular photocatalysts, as has been demonstrated so far.^{12, 18} Another important priority of molecular photocatalyst is the designability of molecular orbitals in order to facilitate transfer and separation of photoexcited charges for the efficient photocatalysis even under visible-light illumination.¹³

On the other hand, semiconductor photocatalysts are advantageous in terms of the band formation.^{8, 15} The band-gap excitation of semiconductors generates multi-electrons and -holes in conduction and valence bands. Therefore, simultaneous multi-electron reduction and oxidation reactions, *e.g.*, overall water splitting¹⁹⁻²² and CO₂ reduction using water as the electron source,¹⁶ have been achieved by a number of semiconductor photocatalysts, while have hardly been reported by using molecular photocatalyst system.²³ In terms of CO₂ reduction, however, semiconductor photocatalysts frequently suffer from the low selectivity of CO₂ reduction by competing efficient proton reduction.¹⁶ Recently, molecular-semiconductor hybrid photocatalysts have been developed to maximize their advantages, although it still remains a challenge for efficient photocatalytic CO₂ reduction.²⁴⁻²⁶

Recently, organic conjugated polymers have emerged as a new candidate of photocatalyst materials.^{27, 28} The organic polymers not only exhibit semiconducting properties due to the extended π -conjugation but also have the molecular designability.²⁹ To date, organic polymer-based photocatalysts have been developed toward CO₂ reduction under visible light.³⁰⁻³⁹ Metal-based catalytic sites^{31, 33-35, 39} are frequently required to selectively reduce CO₂ although some organic

^a Department of Applied Chemistry, Faculty of Science and Engineering, Chuo University, 1-13-27 Kasuga, Bunkyo-ku, Tokyo 112-8551, Japan.
E-mail: nakada.773@g.chuo-u.ac.jp (A.N.), chang@kc.chuo-u.ac.jp (H.C.).

^b Precursory Research for Embryonic Science and Technology (PRESTO), Japan Science and Technology Agency (JST), 4-1-8 Honcho, Kawaguchi, Saitama 332-0012, Japan.

^c Graduate School of Engineering, Toyota Technological Institute, 2-12-1 Hisakata, Tempaku-ku, Nagoya 468-8511, Japan.

^d Waseda Research Institute for Science and Engineering (WISE) and Department of Chemistry and Biochemistry, School of Advanced Science and Engineering, Waseda University, 3-4-1 Okubo, Shinjuku, Tokyo 169-8555, Japan.

^e Department of Applied Chemistry, Graduate School of Engineering, Osaka University, 2-1 Yamadaoka, Suita, Osaka 565-0871, Japan.

^f Department of Graduate School of Engineering, Kyoto University, Katsura, Nishikyo-ku, Kyoto 615-8510, Japan.

^g Waseda Research Institute for Science, Waseda University, 3-4-1 Okubo, Shinjuku, Tokyo 169-8555, Japan.

^h Elements Strategy Initiative for Catalysts & Batteries (ESICB), Kyoto University, 1-30 Goryo-Ohara, Nishikyo-ku, Kyoto 615-8245, Japan.

† Electronic Supplementary Information (ESI) available: [details of any supplementary information available should be included here]. See DOI: 10.1039/x0xx00000x

polymers are reported to facilitate metal-free CO₂ reduction.^{30, 32, 36-38} Hence, design principle, that maximizes the synergy between conjugated skeleton and catalyst moiety, is strongly desired for achieving efficient photocatalytic CO₂ reduction. Several combinations of metal-based catalytic site and organic polymers have been developed so far,^{31, 33-35, 39} while design principle particularly to manipulate the excited charge carrier have not been established satisfactory. Herein, we show strong impacts of excited charge distribution in conjugated polymer photocatalysts with a site-selectively incorporated Ru(II) complex catalyst (Fig. 1a), which are elucidated by combination of ultrafast spectroscopies and theoretical calculation, on their photocatalytic activity for CO₂ reduction.

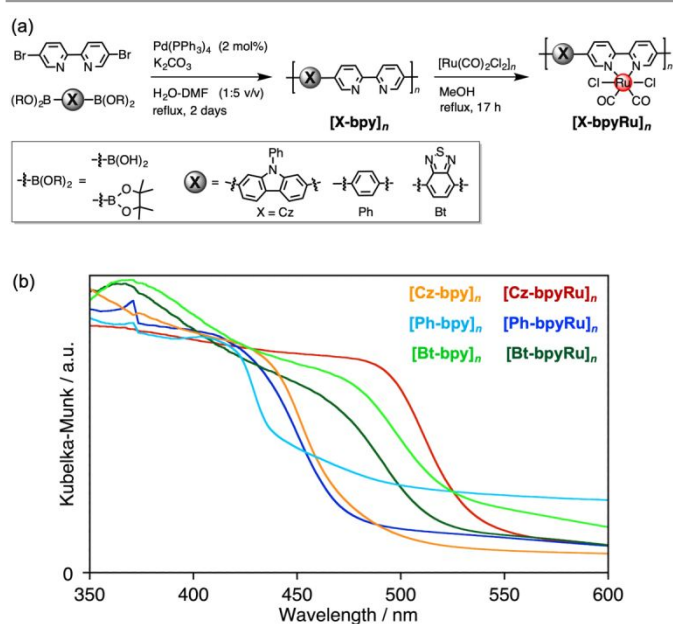


Fig. 1 (a) Synthetic procedures and (b) UV-vis diffuse reflectance spectra of the polymer photocatalysts developed in this study.

Results and discussion

[X-bpy]_n (X = Ph, Bt, and Cz) were synthesized by Suzuki–Miyaura cross-coupling reaction between 5,5'-dibromo-2,2'-bipyridine (Br₂bpy) and diboronate acids or esters corresponding to the X moieties (X-B(OR)₂)₂ with the aid of Pd(PPh₃)₄ catalyst (Fig. 1a). MALDI-TOF-MS spectra of the obtained materials gave repeated peaks with interpeak *m/z* differences corresponding to the X-bpy unit (Fig. S1), indicative of the formation of –[X-bpy]– conjugated networks. The maximum numbers of connected units detected in the MALDI-TOF-MS spectra were 16, 32, and 19 for [Cz-bpy]_n, [Ph-bpy]_n, and [Bt-bpy]_n, respectively. ATR-FT-IR spectra of [X-bpy]_n, which exhibited specific peaks similar with the model monomers corresponding to the X and bpy units, support that the X and bpy skeletons are maintained (Figs. S2-4).

A Ru(II)-complex catalyst moiety was introduced by refluxing [Ru(CO)₂Cl₂]_n and the polymers [X-bpy]_n in methanol. The obtained powder exhibited characteristic CO vibration at 2054 and 1990 cm⁻¹ assignable to the Ru(bpy)(CO)₂Cl₂-type coordination environment regardless of the type of X, indicative of successful post-complexation of the Ru(CO)₂Cl₂ unit to the bipyridine moiety in [X-bpy]_n as the ligand (Figs. S2-4). Based on elemental analyses, the introduced Ru complex moieties were estimated at least ca. 2/3 of the bpy skeleton for all [X-bpyRu]_n. The Ru(II) complex-incorporated polymers are denoted as [X-bpyRu]_n. Scanning electron microscope (SEM) images and XRD patterns suggest that the indefinite low-crystalline structures of the obtained materials (Figs. S5 and S6). We also tried to directly synthesize [Cz-bpyRu]_n by Suzuki–Miyaura cross-coupling between Cz-(B(OR)₂)₂ and as-synthesized Ru(Br₂bpy)(CO)₂Cl₂. However, the CO vibration peaks in IR spectra were shifted to 2019 and 1923 cm⁻¹ after reaction (Fig. S7), suggesting that the Ru(bpy)(CO)₂Cl₂-type coordination environment was not maintained, but formation of a [Ru(bpy)(CO)₂]_n-type network with Ru–Ru bonds.^{40, 41} Therefore, we concluded that the post-complexation method is more suitable for precise synthesis of conjugated polymer with structurally well-defined Ru(II) complex catalyst, and will describe about the post-complexation polymer unless otherwise noted.

In contrast to the colorless building-block monomers (Fig. S8), the obtained polymers exhibited largely red-shifted absorption covering visible region due to the formation of extended π-conjugation (Fig. 1b), as reported for conventional conjugated polymers.^{27, 28} The band positions for each material, which were estimated by the bandgaps (*E_g*) and the ionization energies determined by means of photoelectron yield spectroscopy (PYS),⁴² are shown in Fig. 2. Focusing on the Ru non-incorporated materials, electron-deficient Bt (*E_g* = 2.25 eV) and electron-rich Cz (*E_g* = 2.56 eV) made impacts for narrowing bandgaps compared with [Ph-bpy]_n (*E_g* = 2.69 eV).

To gain further insights on the roles of X moieties for the electron transition, we conducted theoretical calculation of molecular orbitals for the model monomers X-bpy (Fig. 2). Regardless of the X moiety, the frontier orbitals locate around π-conjugated skeletons. The π-π*-based HOMO-LUMO distribution shows, however, different nature depending on the X moiety. In the cases of Ph-bpy, both HOMO and LUMO are delocalized on whole conjugated skeleton. In contrast, charge-transfer characters can be found in the HOMO-LUMO electron transition in the cases of X = Cz and Bt, but the roles of Cz and Bt are different. The electron-rich Cz in Cz-bpy appeared to be HOMO for donating electron to the bpy unit, whereas electron-deficient Bt serves as an acceptor (*i.e.*, LUMO in Bt-bpy). The character of donor-acceptor charge transfer should decrease the *E_g* values of [Cz-bpy]_n and [Bt-bpy]_n, in which the electron donating Cz increases the HOMO energy while the electron withdrawing Bt decrease the LUMO energy, respectively.

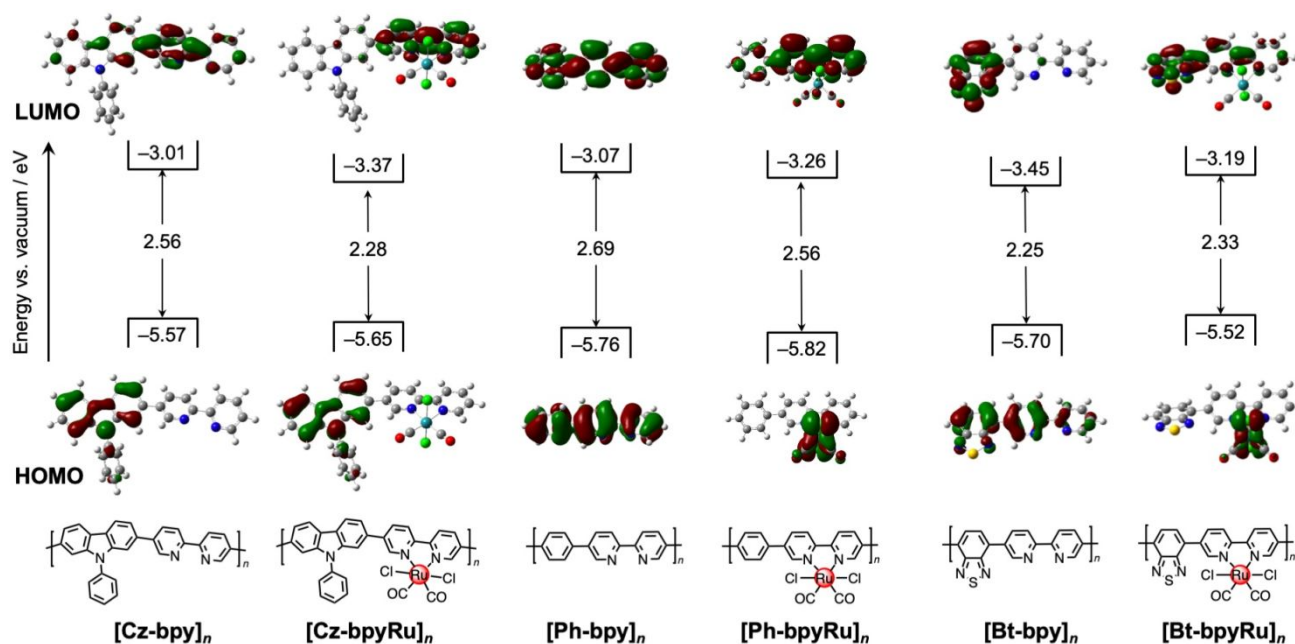


Fig. 2 Experimentally-estimated band positions of $[X\text{-bpyM}]_n$ ($X = \text{Cz, Ph, and Bt}$; $M = \text{none and Ru}$) along with calculated HOMO (lower) and LUMO (upper) distributions of $X\text{-bpyM}$.

Notably, introduction of the Ru(II) complex unit further modified HOMO-LUMO potentials of the polymers. In the case of $X = \text{Ph}$, LUMO energies were decreased with a slight decreased bandgap (ca. 0.1 eV) by introducing the Ru(II) complex. Since LUMOs are delocalized over the whole π -conjugated system in **Ph-bpy** and **Ph-bpyRu** (Fig. 2), this potential shift can be understood by stabilization of the π -conjugated system through coordination of the bpy moiety to the Ru(II) center.⁴³ At a glance, the $X = \text{Cz}$ system exhibits a similar trend with that of $X = \text{Ph}$, whereas a larger degree of bandgap narrowing from **[Cz-bpy]_n** ($E_g = 2.6$ eV) to **[Cz-bpyRu]_n** ($E_g = 2.3$ eV) was obviously observed as a specific feature of the $X = \text{Cz}$ system (Fig. 2). The HOMO and LUMO of **Cz-bpyRu** separately distribute at Cz and bpy moieties, respectively. Therefore, LUMO localized on bpy was selectively stabilized by coordination to the Ru(II) center, leading to decreased bandgap in the case of **[Cz-bpyRu]_n**. Interestingly, introducing the Ru(II) complex to **[Bt-bpy]_n** increased both HOMO-LUMO energies with a slightly expanded bandgap (Fig. 2). The Ru d orbitals participated in the formation of HOMO of **Bt-bpyRu**, in contrast to the $X = \text{Cz}$ system of which both HOMO-LUMO are constructed by the organic conjugated chain without direct contribution of Ru d orbitals. The different origin of HOMO between **Bt-bpy** (π orbitals) and **Bt-bpyRu** (Ru d orbitals) might elevate the HOMO level by introducing the Ru(II) complex moiety, although the reason for the destabilization of LUMO by introducing the Ru(II) complex moiety is unclear at this stage. From these results, we can conclude that the opposite trends in the HOMO-LUMO shifts when introducing the Ru(II) complex moiety are caused by electron donating or withdrawing nature of the unit X. The photoexcited charge distribution for $X\text{-bpyRu}$ was evaluated by the differential Mulliken population between ground and excited states. The differential charges on the bpyRu moiety were -0.057 , 0.001 , and 0.021 for **Cz-bpyRu**, **Ph-bpyRu**, and **Bt-**

bpyRu, respectively (Table S1). These results suggest that **Cz-bpyRu** generates photoexcited electrons relatively located on the bpyRu moiety, while **Bt-bpyRu** generates it on the opposite side. As mentioned in Introduction, not only HOMO-LUMO gap but also its potential and spatial distribution are important to manipulate photoexcited charge carriers to be effectively utilized at the catalytic moiety. Thus, the direct or indirect cooperation of π -conjugated system and metal d-orbitals will expand the tunability of HOMO-LUMO level, gap, and distribution for development of suitable photocatalyst materials.

Prior to photocatalysis studies, behaviors of photoexcited carriers in the polymer materials were evaluated by means of transient spectroscopies. Fig. 3 shows transient photoconductivity signals of $[X\text{-bpyM}]_n$, which were obtained by time-resolved microwave conductivity (TRMC) measurements upon laser excitation ($\lambda = 355$ nm). The photoconductivity values $\phi\Sigma\mu$, where ϕ is the quantum efficiency of charge carrier generation and $\Sigma\mu$ is the sum of photogenerated carrier mobilities, is increased within the instrumental time resolution ($\sim 10^{-7}$ s) and then gradually decreased due to charge recombination and/or trapping. The maximum photoconductivity values $\phi\Sigma\mu_{\text{max}}$ ⁴⁴ were similar among three $[X\text{-bpy}]_n$ compounds (compare grey bars in Fig. 3d). Incorporation of Ru(II) complex moiety into the bpy ligand led to decreased $\phi\Sigma\mu_{\text{max}}$ in the case of $X = \text{Cz}$ (Figs. 3a and 3d). Since the main structures of the polymers are maintained by post-complexation of the $\text{Ru}(\text{CO})_2\text{Cl}_2$ unit (Fig. S2-4), the decreased photoconductivity of **[Cz-bpyRu]_n** compared with **[Cz-bpy]_n** is likely due to charge trapping at the Ru(II) complex moiety. Similar phenomenon was observed in the case of $X = \text{Ph}$ although the degree was smaller than that of $X = \text{Cz}$ (Figs. 3b and 3d). In contrast, the **[Bt-bpyM]_n** system showed negligible change in charge trapping by incorporating the Ru complex moiety (Figs. 3c and 3d).

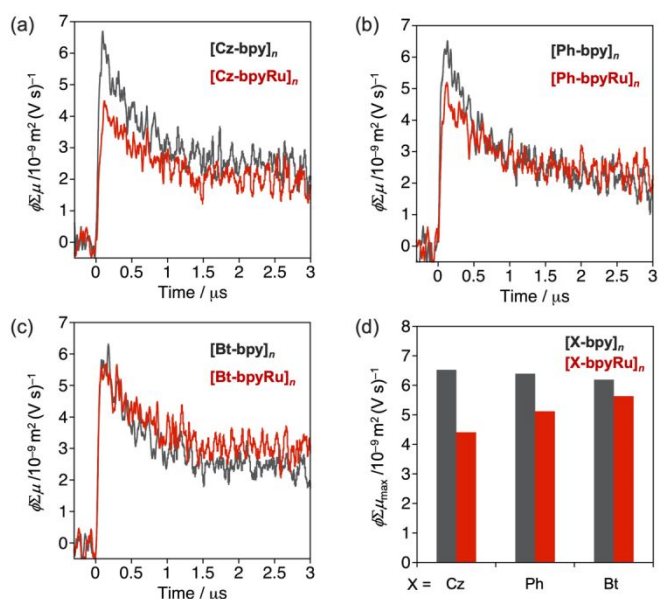


Fig. 3 Transient conductivities of (a) **[Cz-bpyM]_n**, (b) **[Ph-bpyM]_n**, and (c) **[Bt-bpyM]_n** (M = none (grey) or Ru (red)), along with (d) their maximum values ($\phi\Sigma\mu_{\max}$) obtained by photoexcitation at $\lambda = 355$ nm.

For in-depth understanding the origin of photoexcited charge trapping, time-resolved infrared (TR-IR) absorption measurements were conducted. We focused on the characteristic absorption corresponding to the CO vibration in the Ru(bpy)(CO)₂Cl₂ moiety, which reflects the changes in electronic densities at the Ru center.⁴⁵ Upon laser excitation ($\lambda = 420$ nm) to **[Cz-bpyRu]_n**, absorption bands at around 2069 and 2007 cm⁻¹ decreased, whereas lower-energy bands at around 2045 and 1977 cm⁻¹ increased within 1 ps (Fig. 4a). Such a derivative-type differential spectra approximately centered at absorption peaks of the ground state (2060 and 1994 cm⁻¹) are characteristic to the simultaneous decay and rise of the ground state and a new state, respectively.⁴⁶ Kubiak *et al.* reported that one-electron reduction of Ru(bpyR₂)(CO)₂Cl₂ (bpyR₂ = 6,6'-dimethyl-2,2'-bipyridine) induces lower-energy shifts of CO vibration with 25-30 cm⁻¹ owing to the enhanced back donation from the electron-rich Ru center.⁴⁵ Hence, it is strongly suggested that photoexcitation of **[Cz-bpyRu]_n** generates reduced Ru complex moiety through the excited charge trapping. Although **[Ph-bpyRu]_n** and **[Bt-bpyRu]_n** showed similar spectroscopic changes (Figs. 4b and 4c), **[Cz-bpyRu]_n** exhibited the largest generation of the reduced catalyst moiety (Fig. 4d). The trends are in good agreement with those observed in TRMC (*vide supra*, Fig. 3). From aforementioned transient spectroscopies, we can conclude that photoexcited electrons are captured at the Ru(II) complex moiety more effectively in **[Cz-bpyRu]_n** compared with the X = Ph and Bt counterparts, in association with their LUMO distribution at the Ru(II) complex moiety (see Fig. 2).

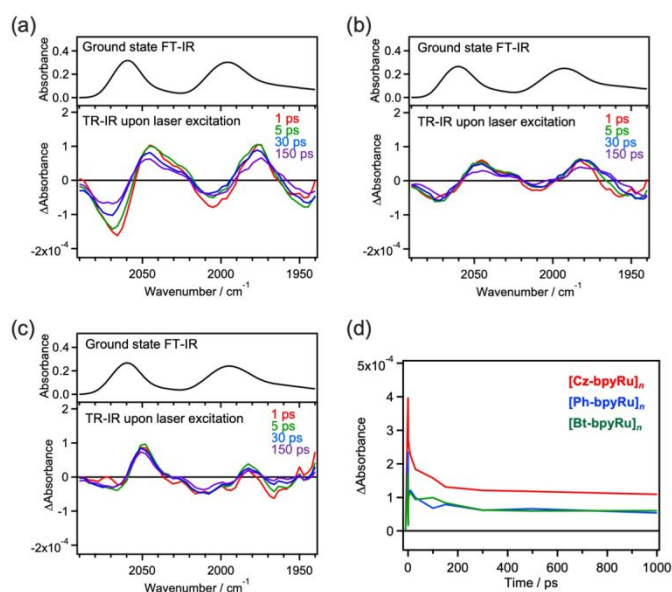


Fig. 4 Ground state FT-IR (upper) and TR-IR (lower) spectra of (a) **[Cz-bpyRu]_n**, (b) **[Ph-bpyRu]_n**, and (c) **[Bt-bpyRu]_n**, along with (d) time courses of the differential absorbance at 2045 cm⁻¹ and 2069 cm⁻¹ (red: **[Cz-bpyRu]_n**, blue: **[Ph-bpyRu]_n**, and green: **[Bt-bpyRu]_n**).

Photocatalytic CO₂ reduction activities of the polymers were evaluated in an MeCN-TEOA (4:1 v/v) dispersion upon visible-light ($\lambda > 400$ nm) irradiation (Table 1). **[Cz-bpyRu]_n** generated formate as the main product together with H₂ and small amount of CO (Fig. 5a and Entry 1 in Table 1). In the absence of photoirradiation, CO₂, or TEOA, almost no photocatalytic activity was found (Entries 2-4, Table 1), indicating that this reaction represents a photochemical reduction of CO₂ using TEOA as an electron donor. By using **[Cz-bpy]_n** instead of **[Cz-bpyRu]_n**, CO₂ reduction products became negligible and the main product switched to H₂ (Entry 5 in Table 1). Therefore, it is strongly suggested that the Ru(II) complex moiety acts as the catalyst for CO₂ reduction. After 12 h photoirradiation, the photocatalysis deactivated (Fig. 5a). In ATR-FT-IR spectra, characteristic CO vibrations corresponding to Ru(bpy)(CO)₂Cl₂-type coordination environment were shifted to 2019 and 1923 cm⁻¹ after photolysis, suggesting that the formation of a [Ru(bpy)(CO)₂]_n-type network with Ru-Ru bonds (Fig. S9). On the other hand, IR spectra corresponding to the organic skeleton was almost unchanged. Hence, we concluded that the changes in Ru catalyst moiety likely cause the deactivation. Although the stability leaves much room for improvement, the wavelength dependency of the formate formation clearly indicates **[Cz-bpyRu]_n** effectively utilizes its HOMO-LUMO photoexcitation even more than 500 nm for photocatalytic reaction (Fig. 5b). Maeda and co-workers reported that copolymerized organic polymers C₃N₄, which were modified with Ru(2,2'-bipyridine-4,4'-diphosphonic acid)(CO)₂Cl₂, facilitate photocatalytic formate formation under $\lambda > 500$ nm visible light, while the quantum efficiency at $\lambda > 500$ nm was not reported.^{47, 48} The external quantum efficiencies of formate formation (EQE_{Formate}) by the present **[Cz-bpyRu]_n** polymer were estimated as 0.44 and 0.38% at 505 and 525 nm, respectively.

These values are comparable or better than that of a triazine-based conjugated polymer for CO formation,³⁰ which is one of the few examples of reliable quantum efficiency at $\lambda > 500$ nm visible light by using organic polymer-based photocatalysts.

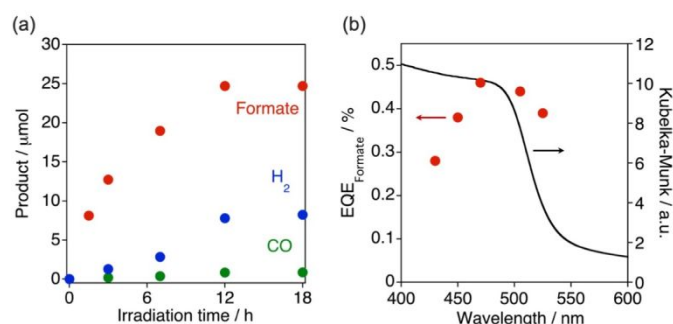


Fig. 5 (a) Time courses of photocatalytic reaction and (b) action spectra of external quantum efficiency of formate formation (EQE_{Formate}) by $[\text{Cz-bpyRu}]_n$ (2 mg) in an MeCN-TEOA (2 mL; 4:1 v/v) dispersion under CO_2 atmosphere.

Table 1. Results of photocatalytic reactions using polymer photocatalysts.^[a]

Entry	Photocatalyst	Control	Product / μmol		
			Formate	CO	H_2
1	$[\text{Cz-bpyRu}]_n$	-[e]	24.7	0.8	7.8
2	$[\text{Cz-bpyRu}]_n$	Without light	N.D.	N.D.	N.D.
3	$[\text{Cz-bpyRu}]_n$	Without CO_2 ^[b]	N.D.	trace	N.D.
4	$[\text{Cz-bpyRu}]_n$	Without TEOA	N.D.	0.5	trace
5	$[\text{Cz-bpy}]_n$	-[e]	0.5	N.D.	26.6
6	$[\text{Ph-bpyRu}]_n$	-[e]	3.6	0.4	0.5
7	$[\text{Bt-bpyRu}]_n$	-[e]	1.7	0.3	0.3

[a] 2 mg of photocatalyst powder in a MeCN-TEOA (2 mL; 4:1 v/v) dispersion was irradiated at $\lambda > 400$ nm for 12 h under a CO_2 atmosphere. [b] Under a N_2 atmosphere.

Notably, $[\text{Cz-bpyRu}]_n$ exhibited 7- to 15-folds higher photocatalytic activity for CO_2 reduction than $[\text{Ph-bpyRu}]_n$ and $[\text{Bt-bpyRu}]_n$ (Entries 6 and 7 in Table 1). Although the bulk structures possibly affect photocatalytic performance, all the $[\text{X-bpyRu}]_n$ polymers have similar indefinite low-crystalline bulk structures (*vide supra*, Figs. S5 and S6). The different visible-light absorbability (Fig. 1) might be a reason of their distinct photocatalytic activities. However, the trend of the formate-formation activity did not change even if a light centered at $\lambda = 430$ nm, where all $[\text{X-bpyRu}]_n$ can enough absorb, was irradiated (Fig. S10). In addition, $[\text{Cz-bpyRu}]_n$ has smaller driving force for both redox reactions than $[\text{Ph-bpyRu}]_n$ (Fig. 2). Therefore, the much better photocatalytic activity of $[\text{Cz-bpyRu}]_n$ most probably be originated from its effective capturing photogenerated electrons at the catalytic Ru(II)-complex moiety as demonstrated by means of transient spectroscopies (Figs. 3 and 4). From these results, we can conclude that precise HOMO-LUMO tuning *via* molecular

engineering with appropriate choice of the building block X in $[\text{X-bpyRu}]_n$ (Cz, Ph, or Bt) enables effective charge trapping at the structurally well-defined Ru(II) complex catalyst unit, leading to the much efficient CO_2 photoreduction.

Conclusions

In this work, we constructed conjugated polymers bearing a Ru(II) complex catalyst in the bipyridine-ligand moiety, and unveiled the relationship between their molecular structure, HOMO-LUMO distribution, excited charge trapping, and photocatalytic activity for CO_2 reduction. Introduction of an electron-donating carbazole skeleton enables LUMO localization and effective trapping photoexcited electrons at the Ru(II) catalyst moiety, engaging in 7- to 15-folds efficient CO_2 reduction compared with phenyl and benzothiadiazole counterparts. Hence, the present study demonstrates the effectiveness of manipulation of local photoexcited charge distributions by the molecular engineering of organic polymers with a site-selectively incorporated molecular catalyst. The carbazole-based polymer $[\text{Cz-bpyRu}]_n$ utilizes visible light at more than 500 nm with a potential photocatalytic efficiency of CO_2 reduction, which is comparable or better than the organic-polymer photocatalyst reported previously.³⁰ On the other side, we should note that the activity of $[\text{Cz-bpyRu}]_n$ has still much room for improvement possibly due to their indefinite low-crystalline bulk structure. Recently, researches on crystal- and pore-structure engineering of organic-polymer photocatalysts including covalent organic frameworks have been accelerated so far.^{28, 33} Therefore, we believe the present strategy of manipulating photoexcited charge carriers expands the opportunity to develop efficient photocatalysts by coupling with well-established bulk engineering.

Experimental

General procedure

^1H NMR (400 MHz) spectra were measured on a Varian 400 spectrometer. Elemental analyses were carried out on a PerkinElmer 2400 II CHN analyzer. UV-vis absorption and diffuse reflectance spectra were recorded at room temperature on Shimadzu U1900i and U2600i spectrophotometers, respectively. Solid-state FT-IR spectra were measured on a Thermo-Fisher Nicolet 6700 spectrometer equipped with a Smart-Orbit (Diamond) attenuated total reflection (ATR) accessory. Solution FT-IR spectra were measured on a JASCO FT/IR-4100 spectrometer. MALDI-TOF-MS spectra were measured on a Shimadzu MALDI-8020 mass spectrometer. Scanning electron microscope (SEM) images were obtained using a Hitachi MC1000 at 10 kV after Pt coating the samples. Powder X-ray diffraction patterns were recorded on a Rigaku Ultima IV diffractometer with $\text{Cu K}\alpha$ radiation. Photoelectron yield spectra (PYS) were measured on a Bunko Keiki BIP-KV202GD apparatus. The PYS measurements provide the lowest ionization energies corresponding to the valence-band maximum potentials.^{42, 49}

Acetonitrile (MeCN; dehydrated, >99.5%), methanol (MeOH; dehydrated, >99.6%), CHCl₃ (>99.0%), CH₂Cl₂ (dehydrated, >99.5%), and K₂CO₃ (>99.5%) were purchased from Kanto Chemical Co. Inc. 5,5-dibromo-2,2'-bipyridine (>98.0%), 9-phenyl-2,7-bis(4,4,5,5-tetramethyl-1,3,2-dioxaborolan-2-yl)-9H-carbazole (>96.0%), 1,4-phenylenediboronic acid, 9-phenylcarbazole (>98.0%), 2,1,3-benzothiadiazole (>99.0%) were purchased from Tokyo Chemical Industry Co., Ltd. Tetrakis(triphenylphosphine)palladium (Pd(PPh₃)₄; >90.0%), triethanolamine (TEOA; >98.0%), *p*-toluenesulfonic acid (>99.0%), ethylenediamine tetraacetic acid (>99.0%), and Bis-Tris (>99.0%) were purchased from Wako Pure Chemical Industries. These materials were used without any further purification. [Ru(CO)₂Cl₂]_n was prepared according to a literature.⁵⁰

Synthesis

Ru(5,5-dibromo-2,2'-bipyridine)(CO)₂Cl₂. A MeOH solution (5 mL) containing [Ru(CO)₂Cl₂]_n (103 mg, 0.45 mmol) and 5,5-dibromo-2,2'-bipyridine (145 mg, 0.46 mmol) in was stirred at reflux for 1 h under N₂ atmosphere. After refluxing, the obtained precipitation was filtered and washed with CHCl₃ (25 mL) for three times giving a pale-yellow powder. Yield 113 mg (0.21 mmol, 46%). ¹H NMR (400 MHz, DMSO-*d*₆): δ = 9.35 (d, *J* = 1.6 Hz), 8.79 (d, *J* = 8.8 Hz), 8.72 (dd, *J* = 8.8, 1.6 Hz). FT-IR (MeOH): ν_{CO} = 2069, 2009 cm⁻¹.

[Cz-bpy]_n. A DMF–H₂O (5:1, v/v; 12 mL) solution containing 5,5'-dibromo-2,2'-bipyridine (314.8 mg, 1.0 mmol), 9-phenyl-2,7-bis(4,4,5,5-tetramethyl-1,3,2-dioxaborolan-2-yl)-9H-carbazole (497.9 mg, 1.0 mmol), K₂CO₃ (1040 mg, 7.5 mmol), and Pd(PPh₃)₄ (23.5 mg, 0.02 mmol) was stirred at reflux for 2 days under a N₂ atmosphere. The obtained precipitate was filtered and washed with water (20 mL), MeOH (20 mL), and CH₂Cl₂ (20 mL). Yield 256 mg.

The same protocol was applied for syntheses of **[Ph-bpy]_n** and **[Bt-bpy]_n** by using 1,4-phenylenediboronic acid and 4,7-bis(4,4,5,5-tetramethyl-1,3,2-dioxaborolan-2-yl)-2,1,3-benzothiadiazole, respectively, as a starting material instead of 9-phenyl-2,7-bis(4,4,5,5-tetramethyl-1,3,2-dioxaborolan-2-yl)-9H-carbazole. Their characterization data are shown in Fig. S1-4.

[Cz-bpyRu]_n. This compound was synthesized *via* two routes.

Route A: A MeOH dispersion (5 mL) containing [Ru(CO)₂Cl₂]_n (22.8 mg, 0.10 mmol) and **[Cz-bpy]_n** (42.9 mg, 0.10 mmol) was refluxed with stirring for 17 h under N₂ atmosphere. After refluxing, the obtained precipitation was filtered and washed with MeOH (20 mL). Yield 62.9 mg. FT-IR (ATR): ν_{CO} = 2054, 1990 cm⁻¹. Elemental analysis Calcd. for C₃₀H₁₉Cl₂N₃O₂Ru (**Cz-bpyRu**): C, 57.61; H, 3.06; N, 6.72. Found: C, 57.50; H, 3.20; N, 6.81.

Route B: A DMF–H₂O (5:1, v/v; 12 mL) solution containing Ru(5,5-dibromo-2,2'-bipyridine)(CO)₂Cl₂ (27.0 mg, 0.05 mmol), 9-phenyl-2,7-bis(4,4,5,5-tetramethyl-1,3,2-dioxaborolan-2-yl)-9H-carbazole (24.8 mg, 0.05 mmol), K₂CO₃ (55.2 mg, 0.40 mmol), and Pd(PPh₃)₄ (1.0 mg, 1 μmol) was stirred at reflux for

2 days under a N₂ atmosphere. The obtained precipitate was filtered and washed with water (20 mL) and MeOH (20 mL). Yield 14.4 mg. FT-IR (ATR): ν_{CO} = 2019, 1923 cm⁻¹.

The same protocol as Route A was applied for syntheses of **[Ph-bpyRu]_n** and **[Bt-bpyRu]_n** by using **[Ph-bpy]_n** and **[Bt-bpy]_n**, respectively, as a starting material instead of **[Cz-bpy]_n**. Elemental analysis Calcd. for C₅₂H₃₆Cl₄N₆O₄Ru₃ (**[Ph-bpyRu]₂[Ph-bpy]₁**): C, 54.18; H, 3.15; N, 7.29. Found: C, 55.16; H, 3.15; N, 7.47. Elemental analysis Calcd. for C₈₈H₅₀Cl₈N₁₀O₈Ru₄S₅ (**[Bt-bpyRu]₄[Bt-bpy]₁**): C, 44.72; H, 2.13; N, 11.85. Found: C, 44.52; H, 2.31; N, 11.82. Further characterization data are shown in Fig. S1-7.

Time-resolved microwave conductivity measurement

Time-resolved microwave conductivity experiments were conducted with the third harmonic generator (THG; 355 nm) of a Nd:YAG laser (Continuum Inc., Surelite II, 5–8 ns pulse duration, 10 Hz) as the excitation source (9.1 × 10¹⁵ photons cm⁻² pulse⁻¹) and X-band microwave (~9.1 GHz) as the probe. The photoconductivity Δσ was obtained by eq 1

$$\Delta\sigma = \Delta P_r / (AP_r) \quad (1)$$

where Δ*P_r*, *A*, and *P_r* are the transient power change of the reflected microwave power, the sensitivity factor, and the reflected microwave power, respectively. The transient photoconductivity Δσ was converted to the product of the quantum yield (φ) and the sum of charge carrier mobilities Σμ by eqs 2 and 3

$$\Sigma\mu = \mu_+ + \mu_- \quad (2)$$

$$\phi\Sigma\mu = \Delta\sigma / (eI_0F_{\text{light}}) \quad (3)$$

where *e* and *F_{light}* are the unit charge of a single electron and a correction (or filling) factor, respectively. The experiments were performed in air at room temperature (298 K).

Time-resolved infrared absorption spectroscopy

The time-resolved infrared absorption measurements were performed with the spectrometer described previously.⁵¹ The powder sample was mixed with KCl powder, pelletized, and set in an IR cell filled with 20 torr N₂. The measurements were carried out by the pump-probe method with a Ti:sapphire regenerative amplifier (Spectra Physics, Solstice, 90 fs duration, 1 kHz repetition rate) and optical parametric amplifiers (OPAs; Spectra Physics, TOPAS Prime). The sample was photoexcited by a 420 nm pulse (0.5 μJ pulse⁻¹, 500 Hz) from the OPA. The probe MIR pulse was generated by the difference frequency generation between the signal and idler from the OPA in an AgGaS₂ crystal, and was detected with a 128-channel linear MCT array detector (Infrared Systems Development, FPAS-0144). The MIR signal was analysed after subtraction of smooth backgrounds from the spectra.

Photocatalytic reactions

An MeCN-TEOA dispersion (2 mL) of **[X-bpyM]_n** (X = Cz, Ph, or Bt; M = none or Ru) was placed in a pyrex test tube (inner diameter: 10 mm; volume: 8.4 mL), degassed with CO₂ or N₂ bubbling (20 min), and sealed by a rubber septum prior to the photoirradiation. The sample tube was placed in a LED merry-go-round apparatus (Iris-MG-S, Cell system inc.) and irradiated

with visible light ($\lambda > 400$ nm) with stirring. The gaseous products *i.e.*, CO and H₂ were analyzed by a Shimadzu GC-2010 gas chromatograph (MS-5A column, Ar carrier) combined with a TCD detector. Formate produced in the liquid phase was analyzed by a Shimadzu LC-20AT HPLC system equipped with two Shimadzu Shim-pack FAST-OA columns (100 × 7.8 mm) and a Shimadzu CDD-10A conductivity detector. An aqueous solution containing *p*-toluenesulfonic acid (0.95 g/L) was used as the eluent at a flow rate of 0.8 mL min⁻¹ (column temperature: 313 K). After column separation, the eluent was mixed with an aqueous solution containing *p*-toluenesulfonic acid (0.95 g/L), ethylenediamine tetraacetic acid (0.03 g/L), and Bis-Tris (4.18 g/L). For wavelength dependency measurements, a LED lamp with independent wavelength centered at 430, 450, 470, 505, or 525 nm (CL-H1 series, Asahi Spectra Co.) was used at a fixed photon flux of 2.1×10^{-7} einstein s⁻¹, instead of aforementioned LED merry-go-round system. The external quantum efficiencies of photocatalytic formate formation (EQE_{Formate}) were determined on the basis of Eq. 4:

$$\text{EQE}^{\text{Formate}} = \frac{n \times \text{Amount of formate produced (mol)}}{\text{Inputted photon (einstein)}} \quad (4)$$

where *n* indicates the numbers of electrons required to generate one molecule of the product (*i.e.*, 2 for formate formation by CO₂ reduction).

Computational details

Geometry optimizations were performed using the density functional theory (DFT) with ωB97X-D exchange-correlation functional.⁵² For core electrons of Ru ([Ar]3d¹⁰), Stuttgart/Dresden pseudopotentials⁵³ at the multi Dirac–Fock level were used. Corresponding double- ζ basis sets were adopted to valence orbitals of Ru. For other elements, namely, C, H, Cl, N, O and S, correlation-consistent basis sets at double- ζ level termed cc-pVDZ^{54, 55} were employed. Harmonic vibrational frequencies were also calculated analytically to confirm whether the optimized structure converge to an equilibrium geometry point. For the optimized structure, single point calculations were performed using time-dependent DFT with the ωB97X-D functional to obtain the electronic structure in the T₁ state. Mulliken atomic charges in the S₀ and T₁ states were evaluated at the S₀ optimized structure. All calculations were performed by Gaussian 09 program.⁵⁶

Conflicts of interest

There are no conflicts to declare.

Acknowledgements

This work was supported by JST PRESTO grant JPMJPR20T5 (Controlled Reaction), by JSPS KAKENHI grants JP19K23652 and JP19H02736 as well as by MEXT KAKENHI grants JP20H05113 (I⁴LEC) and JP18H05517 (Hydrogenomics), and by the Research Promotion Fund from the Promotion and Mutual Aid Corporation for Private Schools of Japan.

Notes and references

1. C. A. Trickett, A. Helal, B. A. Al-Maythaly, Z. H. Yamani, K. E. Cordova and O. M. Yaghi, *Nat. Rev. Mater.*, 2017, **2**, 17045.
2. Y. Zheng, W. Zhang, Y. Li, J. Chen, B. Yu, J. Wang, L. Zhang and J. Zhang, *Nano Energy*, 2017, **40**, 512-539.
3. A. M. Appel, J. E. Bercaw, A. B. Bocarsly, H. Dobbek, D. L. DuBois, M. Dupuis, J. G. Ferry, E. Fujita, R. Hille, P. J. Kenis, C. A. Kerfeld, R. H. Morris, C. H. Peden, A. R. Portis, S. W. Ragsdale, T. B. Rauchfuss, J. N. Reek, L. C. Seefeldt, R. K. Thauer and G. L. Waldrop, *Chem. Rev.*, 2013, **113**, 6621-6658.
4. J. Artz, T. E. Müller, K. Thenert, J. Kleinekorte, R. Meys, A. Sternberg, A. Bardow and W. Leitner, *Chem. Rev.*, 2018, **118**, 434-504.
5. D. T. Whipple and P. J. A. Kenis, *J. Phys. Chem. Lett.*, 2010, **1**, 3451-3458.
6. C. Costentin, M. Robert and J. M. Saveant, *Chem. Soc. Rev.*, 2013, **42**, 2423-2436.
7. S. C. Roy, O. K. Varghese, M. Paulose and C. A. Grimes, *ACS Nano*, 2010, **4**, 1259-1278.
8. J. L. White, M. F. Baruch, J. E. Pander, Y. Hu, I. C. Fortmeyer, J. E. Park, T. Zhang, K. Liao, J. Gu, Y. Yan, T. W. Shaw, E. Abelev and A. B. Bocarsly, *Chem. Rev.*, 2015, **115**, 12888-12935.
9. C. Song, *Catal. Today*, 2006, **115**, 2-32.
10. G. Centi and S. Perathoner, *Catal. Today*, 2009, **148**, 191-205.
11. O. S. Bushuyev, P. De Luna, C. T. Dinh, L. Tao, G. Saur, J. van de Lagemaat, S. O. Kelley and E. H. Sargent, *Joule*, 2018, **2**, 825-832.
12. A. J. Morris, G. J. Meyer and E. Fujita, *Acc. Chem. Res.*, 2009, **42**, 1983-1994.
13. Y. Yamazaki, H. Takeda and O. Ishitani, *J. Photochem. Photobiol. C*, 2015, **25**, 106-137.
14. S. N. Habisreutinger, L. Schmidt-Mende and J. K. Stolarczyk, *Angew. Chem. Int. Ed.*, 2013, **52**, 7372-7408.
15. Y. Ma, X. Wang, Y. Jia, X. Chen, H. Han and C. Li, *Chem. Rev.*, 2014, **114**, 9987-10043.
16. S. Yoshino, T. Takayama, Y. Yamaguchi, A. Iwase and A. Kudo, *Acc. Chem. Res.*, 2022, **55**, 966-977.
17. H. Kageyama, K. Hayashi, K. Maeda, J. P. Atfield, Z. Hiroi, J. M. Rondinelli and K. R. Poeppelmeier, *Nat. Commun.*, 2018, **9**, 772.
18. H. Takeda, C. Cometto, O. Ishitani and M. Robert, *ACS Catal.*, 2016, **7**, 70-88.
19. Q. Wang and K. Domen, *Chem. Rev.*, 2020, **120**, 919-985.
20. K. Maeda, *Phys. Chem. Chem. Phys.*, 2013, **15**, 10537-10548.
21. Y. Wang, H. Suzuki, J. Xie, O. Tomita, D. J. Martin, M. Higashi, D. Kong, R. Abe and J. Tang, *Chem. Rev.*, 2018, **118**, 5201-5241.
22. F. E. Osterloh, *Chem. Soc. Rev.*, 2013, **42**, 2294-2320.
23. Y. H. Hong, Y. M. Lee, W. Nam and S. Fukuzumi, *J. Am. Chem. Soc.*, 2022, **144**, 695-700.
24. K. E. Dalle, J. Warnan, J. J. Leung, B. Reuillard, S. Isabell and E. Reisner, *Chem. Rev.*, 2019, **119**, 2752-2875.
25. T. Morikawa, S. Sato, K. Sekizawa, T. M. Suzuki and T. Arai, *Acc. Chem. Res.*, 2022, **55**, 933-943.
26. A. Nakada, H. Kumagai, M. Robert, O. Ishitani and K. Maeda, *Acc. Mater. Res.*, 2021, **2**, 458-470.

27. C. Dai and B. Liu, *Energy Environ. Sci.*, 2020, **13**, 24-52.
28. J. M. Lee and A. I. Cooper, *Chem. Rev.*, 2020, **120**, 2171-2214.
29. Y. Wang, A. Vogel, M. Sachs, R. S. Sprick, L. Wilbraham, S. J. A. Moniz, R. Godin, M. A. Zwijnenburg, J. R. Durrant, A. I. Cooper and J. Tang, *Nat. Energy*, 2019, **4**, 746-760.
30. C. Yang, W. Huang, L. C. da Silva, K. A. I. Zhang and X. Wang, *Chem. Eur. J.*, 2018, **24**, 17454-17458.
31. H.-P. Liang, A. Acharjya, D. A. Anito, S. Vogl, T.-X. Wang, A. Thomas and B.-H. Han, *ACS Catal.*, 2019, **9**, 3959-3968.
32. X. Yu, Z. Yang, B. Qiu, S. Guo, P. Yang, B. Yu, H. Zhang, Y. Zhao, X. Yang, B. Han and Z. Liu, *Angew. Chem. Int. Ed.*, 2019, **58**, 632-636.
33. Z. Fu, X. Wang, A. M. Gardner, X. Wang, S. Y. Chong, G. Neri, A. J. Cowan, L. Liu, X. Li, A. Vogel, R. Clowes, M. Bilton, L. Chen, R. S. Sprick and A. I. Cooper, *Chem. Sci.*, 2020, **11**, 543-550.
34. X. Y. Dong, Y. N. Si, Q. Y. Wang, S. Wang and S. Q. Zang, *Adv. Mater.*, 2021, **33**, 2101568.
35. J. Li, K. Ma, Y. He, S. Ren, C. Li, X.-B. Chen, Z. Shi and S. Feng, *Catal. Sci. Tech.*, 2021, **11**, 7300-7306.
36. G. E. M. Schukraft, R. T. Woodward, S. Kumar, M. Sachs, S. Eslava and C. Petit, *ChemSusChem*, 2021, **14**, 1720-1727.
37. L. Hou, G. Tang, H. Huang, S. Yin, B. Long, A. Ali, G.-J. Deng and T. Song, *J. Mater. Chem. A*, 2022, **10**, 5287-5294.
38. S. Barman, A. Singh, F. A. Rahimi and T. K. Maji, *J. Am. Chem. Soc.*, 2021, **143**, 16284-16292.
39. R. Kuriki and K. Maeda, *Phys. Chem. Chem. Phys.*, 2017, **19**, 4938-4950.
40. G. Gerbaud, J. M. Mouesca, S. Hediger, S. Chardon-Noblat, F. Lafalet, A. Deronzier and M. Bardet, *Phys. Chem. Chem. Phys.*, 2010, **12**, 15428-15435.
41. Y. Tamaki, T. Morimoto, K. Koike and O. Ishitani, *Proc. Natl. Acad. Sci. USA*, 2012, **109**, 15673-15678.
42. Y. Nakayama, S. Machida, D. Tsunami, Y. Kimura, M. Niwano, Y. Noguchi and H. Ishii, *Appl. Phys. Lett.*, 2008, **92**, 153306.
43. A. A. Vlček, *Coord. Chem. Rev.*, 1982, **43**, 39-62.
44. A. Saeki, S. Yoshikawa, M. Tsuji, Y. Koizumi, M. Ide, C. Vijayakumar and S. Seki, *J. Am. Chem. Soc.*, 2012, **134**, 19035-19042.
45. C. W. Machan, M. D. Sampson and C. P. Kubiak, *J. Am. Chem. Soc.*, 2015, **137**, 8564-8571.
46. A. Yamakata, T.-a. Ishibashi and H. Onishi, *Bull. Chem. Soc. Jpn.*, 2002, **75**, 1019-1022.
47. K. Shibata, K. Kato, C. Tsounis, T. Kanazawa, D. Lu, S. Nozawa, A. Yamakata, O. Ishitani and K. Maeda, *Solar RRL*, 2019, **4**, 1900461.
48. C. Tsounis, R. Kuriki, K. Shibata, J. J. M. Vequizo, D. Lu, A. Yamakata, O. Ishitani, R. Amal and K. Maeda, *ACS Sustain. Chem. Eng.*, 2018, **6**, 15333-15340.
49. A. Nakada, M. Higashi, T. Kimura, H. Suzuki, D. Kato, H. Okajima, T. Yamamoto, A. Saeki, H. Kageyama and R. Abe, *Chem. Mater.*, 2019, **31**, 3419-3429.
50. P. A. Anderson, G. B. Deacon, K. H. Haarmann, F. R. Keene, T. J. Meyer, D. A. Reitsma, B. W. Skelton, G. F. Strouse, N. C. Thomas, J. A. Treadway and A. H. White, *Inorg. Chem.*, 1995, **34**, 6145-6157.
51. A. Yamakata, M. Kawaguchi, N. Nishimura, T. Minegishi, J. Kubota and K. Domen, *J. Phys. Chem. C*, 2014, **118**, 23897-23906.
52. J.-D. Chai and M. Head-Gordon, *Phys. Chem. Chem. Phys.*, 2008, **10**, 6615-6620.
53. K. A. Peterson, D. Figgen, M. Dolg and H. Stoll, *J. Chem. Phys.*, 2007, **126**, 124101-124112.
54. T. H. Dunning, *J. Chem. Phys.*, 1989, **90**, 1007-1023.
55. D. E. Woon and T. H. Dunning, *J. Chem. Phys.*, 1993, **98**, 1358-1371.
56. M. J. Frisch, G. W. Trucks, H. B. Schlegel, G. E. Scuseria, M. A. Robb, J. R. Cheeseman, G. Scalmani, V. Barone, B. Mennucci, G. A. Petersson, H. Nakatsuji, M. Caricato, X. Li, H. P. Hratchian, A. F. Izmaylov, J. Bloino, G. Zheng, J. L. Sonnenberg, M. Hada, M. Ehara, K. Toyota, R. Fukuda, J. Hasegawa, M. Ishida, T. Nakajima, Y. Honda, O. Kitao, H. Nakai, T. Vreven, J. A. Montgomery Jr, J. E. Peralta, F. Ogliaro, M. Bearpark, J. J. Heyd, E. Brothers, K. N. Kudin, V. N. Staroverov, T. Keith, R. Kobayashi, J. Normand, K. Raghavachari, M. Klene, J. E. Knox, J. B. Cross, V. Bakken, C. Adamo, J. Jaramillo, R. Gomperts, R. E. Stratmann, O. Yazyev, A. J. Austin, R. Cammi, C. Pomelli, J. W. Ochterski, R. L. Martin, K. Morokuma, V. G. Zakrzewski, G. A. Voth, P. Salvador, J. J. Dannenberg, S. Dapprich, A. D. Daniels, O. Farkas, J. B. Foresman, J. V. Ortiz, J. Cioslowski and D. J. Fox, *Gaussian 09, Rev. C.01*, Gaussian, Inc., Wallingford, CT, 2010.